

In-situ nitrogen fate in the vadose zone of different soil types and its implications for groundwater quality in the Huaihe River Basin, China

Rongfu Li^{1,2} · Xiaohong Ruan^{1,2} · Tianhai Ma³ · Ying Bai^{1,2} · Congqiang Liu⁴

Received: 2 March 2020 / Revised: 9 March 2020 / Accepted: 17 March 2020 / Published online: 28 April 2020
© Science Press and Institute of Geochemistry, CAS and Springer-Verlag GmbH Germany, part of Springer Nature 2020

Abstract This paper focused on nitrate fate in the vadose zone (VZ) and its implications for groundwater vulnerability under different soil types in the agricultural area of Huaihe River Basin, China. Isotopic compositions of nitrate ($\delta^{15}\text{N}$ and $\delta^{18}\text{O}$) along with NO_3^- and Cl^- concentrations were determined in the VZ-shallow groundwater continuum beneath silty-loam and silty-clay-loam, which are distinctive in texture and organic carbon (OC). In the soil zone (< 1 m in depth), measured $\delta^{18}\text{O}-\text{NO}_3^-$ suggested the ubiquitous of nitrification regardless of soil types. In the subsoil zone (> 1 m in depth), however, the concurrent enrichment of $\delta^{15}\text{N}-\text{NO}_3^-$ and $\delta^{18}\text{O}-\text{NO}_3^-$ indicated the occurrence of denitrification, which showed a dependence on subsoil properties. Specifically, during wheat and maize land uses, denitrification removed as much as 76 %–88 % of the total nitrate where the subsoil was dominated by stratified OC-rich silty-clay-loam. In contrast, only 0 %–28 % of the nitrate was degraded via denitrification where the subsoil was composed of uniform, OC-depleted silty-loam. Furthermore, inactive denitrification and higher permeability in the silty-loam VZ implied

higher groundwater vulnerability. This observation was consistent with the fact that groundwater NO_3^- -N concentration beneath silty-loam (11.24 mg L^{-1}) was over two times higher than that of the silty-clay-loam (5.32 mg L^{-1}), where stricter fertilization management and conservation strategies should be applied to protect groundwater quality.

Keywords Vadose zone · Silty-loam · Silty-clay-loam · Nitrogen transformation · Groundwater vulnerability · Stable isotopes

1 Introduction

Excessive use of agricultural nitrogen (N) fertilizer has resulted in the dramatic increase of nitrate accumulation in soil profiles (Ascott et al. 2017), groundwater (Gu et al. 2013), and surface water (Donner and Kucharik 2003), and thus resulted in a global environmental concern (Rivett et al. 2008). Vadose zone (VZ) is an important pathway for topsoil N to transport from the land surface into the aquifer and plays a critical role in N storage (Ascott et al. 2017) and transformations (Holden and Fierer 2005). As such, a clear understanding of N behavior in the VZ will facilitate the understanding of groundwater vulnerability for nitrate pollution.

For the biogeochemical transformations of N in the VZ, numerous laboratory soil incubations have been carried out to explore N transformation microorganism (Holden and Fierer 2005), and kinetics such as mineralization (Bonde and Lindberg 1988), nitrification (Koper et al. 2010), denitrification (Liu et al. 2010), and anammox (Zhu et al. 2018). For N transport and leaching processes in the VZ, the most commonly used methods were soil-column

✉ Xiaohong Ruan
ruanxh@nju.edu.cn

Congqiang Liu
liucqiang@vip.skleg.cn

¹ MOE Key Laboratory of Surficial Geochemistry, Nanjing University, Nanjing 210023, China

² Department of Water Science, School of Earth Sciences and Engineering, Nanjing University, Nanjing 210023, China

³ Jinling Institute of Nanjing University, Nanjing 210089, China

⁴ Institute of Surface-Earth System Science, Tianjin University, Tianjin 300072, China

experiment (González-Delgado and Shukla 2011) and lysimeters (Rasse et al. 2000). However, these laboratory studies provide no insights into the in-situ behavior of N, and soil-column/lysimeters rarely cover the entire VZ, and thus could not provide a full understanding of the in-situ N fate in the VZ and its impact on groundwater.

One of the strategies to overcome the deficiency of laboratory studies is to carry out field observations using the stable isotopic technique (Singh et al. 2018; Stummpp et al. 2018). Based on the dual-isotopic signature of nitrate ($\delta^{15}\text{N}$ and $\delta^{18}\text{O}$) and the isotopic fractionation, the major N transformation pathways in the VZ and N sources in the groundwater could be traced in-situ (Denk et al. 2017). This method was proved robust under various environments, such as croplands (McMahon et al. 2006), waste lagoons (Baram et al. 2012), riparian zone (Yuan et al. 2012), alluvial deposits (Izbicki et al. 2015), and Loess Plateau (Jia et al. 2018). These studies have revealed that N fate in the VZ was mainly controlled by N inputs and irrigation regimes, climatic conditions, and VZ material properties such as carbon and nitrogen availability, soil particle size fractionation, and texture.

China is dependent on agricultural production and numerous soil types are used for this purpose, including 12 orders, 30 suborders, 60 groups according to the *Classification and Codes for Chinese Soil* (GB 17296-2009). Past work on VZ N behavior of the agricultural area mainly focused on limited soil types such as alluvial deposits (Yuan et al. 2012), sandy-silt and silty-sand (Zhang et al. 2012), and Loess Plateau (Jia et al. 2018). These previous studies have suggested high denitrification potential in fine-particle alluvial deposits, while denitrification was rare in the VZ with coarse particle size. Due to the great complexity and site-specificity of climate, soils, biomass, parent material, and soil-forming processes (Gray et al. 2011; Bünenmann et al. 2018), an in-situ assessment on N fate in the VZ and its impact on groundwater under integrated soil and climatic conditions is essential to better reveal groundwater vulnerability and appropriate land management practices.

In the present study, we attempt to examine the fate of VZ N and its implications for groundwater vulnerability beneath two representative soil types, Fluvo-aquic Soil (FAS) and Lime-concretion Black Soil (LCBS). These two soil types make up 34 % and 13 % respectively of the total arable land in the Huaihe River Basin, the stratification and OC contents of the LCBS is substantially different to that of the FAS (Fig. 1a). Multi-isotope technique was used to trace the in-situ N transformation pathways. It was found that the uniform, OC-depleted silty-loam (FAS) did not support the denitrification process in the subsoil zone below 1 m, resulting in higher groundwater vulnerability,

which could provide rational guidance for improved fertilization under different soil types.

2 Materials and methods

2.1 Study area and sampling methods

The Huaihe River Basin (HRB) is one of the core agricultural areas in China, with major crop types of maize and wheat rotation. The HRB accounts for 17 % of the national grain production using 10 % of the national arable land, which has been achieved through substantial increases in the use of synthetic fertilizers of urea, ammonium phosphate, and potassium sulfate containing N, P, and K as high as ~ 650 , 110, and 50 kg ha^{-1} year $^{-1}$. Chemical fertilizer was mainly applied in June and October when maize and wheat were drilled.

Fluvo-aquic Soil (FAS, site A) is semi-hydro morphic soil developed from alluvial sediment with a homogeneous silty-loam parent and is depleted with OC. In contrast, Lime-concretion Black Soil (LCBS, site B) is a river or lake alluvial deposit composed of a major silty-loam parent with interbedded silty-clay-loam, which is richer in clay (Fig. 1b, c). According to the hydrogeological boreholes to the depth of ~ 12 m, the first aquifers beneath the VZ at both sites were mainly composed of sandy clay loam, with a buried depth of 3.1–5.2 m and 3.5–7.5 m (Fig. 1c). The lower confining bed was an impermeable clay/silty-clay stratum with a thickness of ~ 6.2 and ~ 4.5 m.

Annual precipitation and mean pan evaporation in the study area were 862.5 and 1008.3 mm (<https://yc.wsj.net/ahsxx/LOL/public/public.html>), with 50 %–80 % of the precipitation falls during maize land use (from June to September) (Fig. 1d). Depth to the water table at both sites was about 2.6 m in June, and was 2.7 and 2.2 m at site A and site B in September.

Soil-core sampling was conducted after the harvest of wheat (June) and maize (September) in 2014, representing the wheat land use (WLU) and the maize land use (MLU), respectively. A total of four soil cores were drilled using a 7.5 cm diameter hollow stem hand auger from land surface to the water table in silty-loam and silty-clay-loam areas (Fig. 1a). Soil and subsoil were sampled continuously with an interval of 10 cm, homogenized, and sealed in polyethylene bags.

Groundwater from the first aquifers below the VZ was collected from completely penetrating wells with a screening depth of ~ 10 m around the soil sampling sites (< 50 m in distance). A total of 18 groundwater samples were collected from two and seven wells in site A and B respectively during the wheat and maize land uses. Before groundwater sampling, old water in the wells was pumped

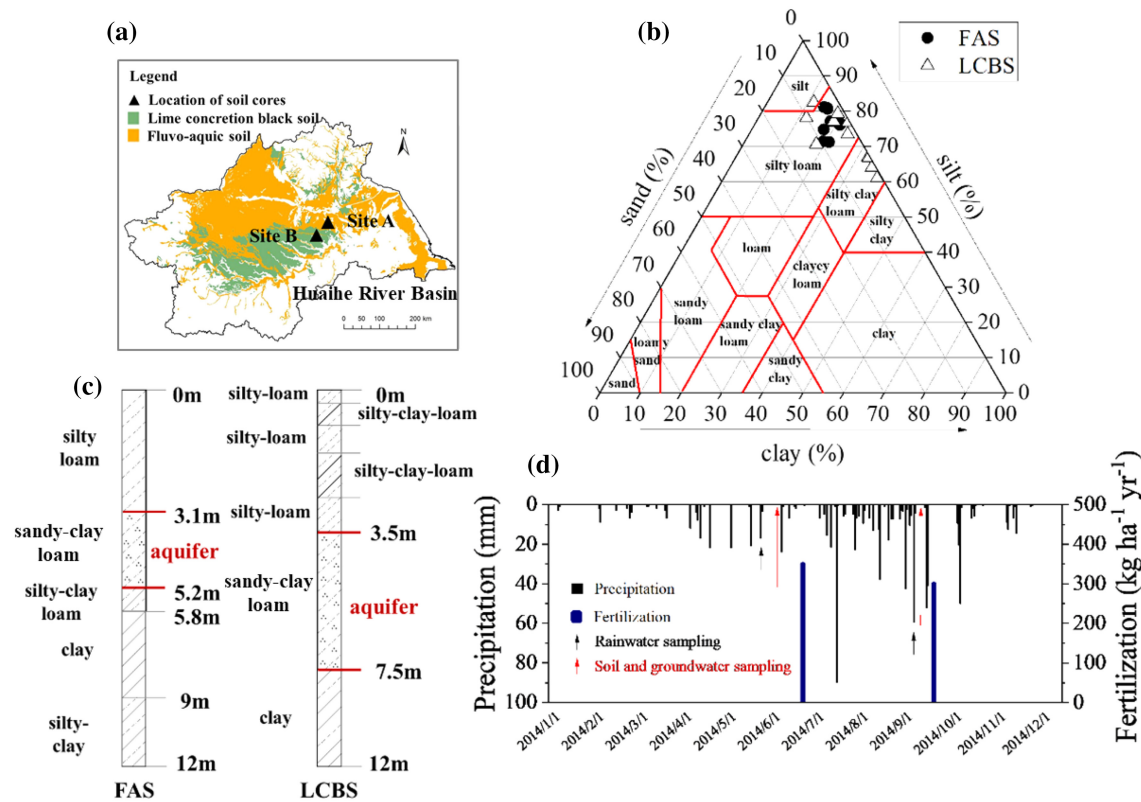


Fig. 1 **a** Main soil types distribution, and sampling sites in the Huaihe River Basin, **b** VZ soil particle fractionation classification for Fluvo-aquic soil (FAS) and Lime concretion black soil (LCBS) according to *soil classification of United States Department of Agriculture (USDA)*, **c** hydrogeological profiles of VZ-groundwater for FAS and LCBS from land surface to the depth of 12 m, **d** precipitation, fertilization, and sampling time during the study period

out to collect freshwater as much as possible. Groundwater parameters such as temperature (T), electrical conductivity (EC), pH, oxidation-reduction potential (ORP), and dissolved oxygen (DO) were continuously monitored during pumping using a multi-parameter water quality instrument (YSI ProPlus, USA). Groundwater samples were collected after the values of these parameters became constant. Two rainwater samples were collected during the rainfall event before soil-core and groundwater sampling (Fig. 1d). All VZ materials, groundwater, and rainwater samples were placed in an icebox immediately and analyzed within 24 h.

2.2 Analytical methods

A minimum of 100 g of VZ material was dried at 105 °C for 12 h to determine the gravimetric moisture content (θ_g). VZ water extracts were obtained following the method described by Yuan et al. (2012). Briefly, 200 g of VZ material was mixed with 200 mL of fresh deionized water, shaken for 30 min at room temperature, centrifuged at a rotation speed of 4000 rpm for 10 min, and then filtered through 0.22-μm cellulose-acetate filters. The rest of the

VZ material was air-dried, ground, sieved (200 mesh), and used for physicochemical parameters determination.

Anions (NO_3^- and Cl^-) of VZ water extract, rainwater, and groundwater were analyzed by the ion chromatography (ICS-2000, Dionex, USA). VZ material particle size fractionation was determined by a laser scattering particle size analyzer (NANOSAQLA, Japan). Total nitrogen (TN) of the VZ materials was measured by the Kjeldahl method (BUCHI K-350 unit, Switzerland), and organic carbon (OC) was determined by the elemental analyzer (Flash Smart, Thermo Fisher, USA). Pore-water ion concentrations ($C_{\text{pore-water}}$) in the VZ were calculated based on $C_{\text{pore-water}} = C_{\text{extract}} \times \frac{1+\theta_g}{\theta_g}$, where C_{extract} is ion concentration in the VZ water extracts, and θ_g is the VZ material gravimetric moisture content.

The stable isotopic compositions of rainwater and groundwater (δD and $\delta^{18}\text{O}$, expressed as $\delta(\text{‰}) = \left(\frac{R_{\text{sample}}}{R_{\text{standard}}} - 1 \right) \times 1000$) were obtained using a Finnigan (MAT-253). The $\delta^{15}\text{N}$ and $\delta^{18}\text{O}$ of NO_3^- were measured by an isotope ratio mass spectrometer (IsoPrime, GV, UK) using the “denitrifier method” (Sigman et al. 2001; Casciotti et al. 2002). Four international nitrate

standards (USGS-32, USGS-34, USGS-35, and IAEA-N3) were used to calibrate the measured $\delta^{15}\text{N}$ and $\delta^{18}\text{O}$ data. Each sample was measured in triplicate. The Vienna standard mean ocean water (VSMOW) was used as the reference for D/H and $^{18}\text{O}/^{16}\text{O}$ ratios, whereas average N_2 in the air was used to determine $^{15}\text{N}/^{14}\text{N}$ ratios.

3 Results

3.1 Physical and chemical characteristics of VZ materials

The FAS has a silty loam soil texture in the entire VZ, and the content of clay varied within a narrow range ($18.4\% \pm 2.3\%$). In contrast, the LCBS has layers of silty loam texture (0–0.4, 1.0–1.4, and 1.8–2.4 m) and silty clay loam texture layers (0.4–0.8, and 1.4–1.8 m) (Fig. 2a, b). The clay content in the silty clay loam layers (34.4 % \pm 2.2 %) of LCBS was significantly higher ($p < 0.001$, t test) than that in the corresponding depth of FAS profile (17.5 % \pm 2.6 %). Moreover, VZ material of silty-clay-loam was richer in TN ($0.04\% \pm 0.02\%$) and OC ($1.97\% \pm 0.39\%$), which were two-fold, and 2.5-fold higher than those ($0.02\% \pm 0.01\%$, and $0.79\% \pm 0.34\%$) of silty-loam (Fig. 2c, d).

In the homogeneous VZ of silty-loam, measured θ_g varied remarkably down the vertical profile (0.18 ± 0.05 in WLU and 0.20 ± 0.03 in MLU) (Fig. 3a). In contrast, θ_g in the stratified VZ of silty-clay-loam showed less vertical variations (0.17 ± 0.02 in WLU and 0.19 ± 0.01 in MLU) (Fig. 4a). Moreover, in the VZ of both sites, measured θ_g during MLU was higher than that of WLU, which could be explained by higher precipitation during MLU (Fig. 1d).

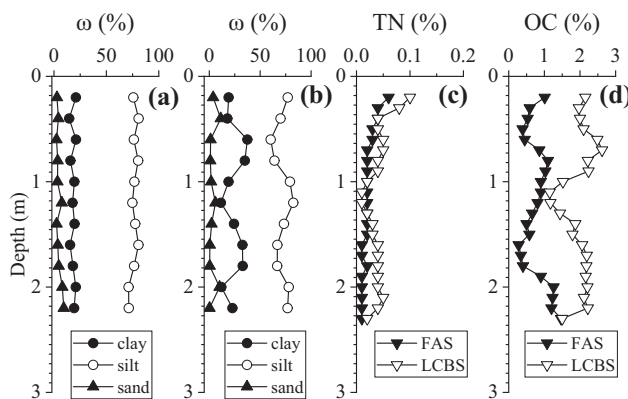


Fig. 2 **a, b** profiles of VZ material particle size fractionation of FAS and LCBS, **c** total nitrogen content, and **d** organic carbon content

3.2 Nitrate and chloride concentrations in VZ and groundwater

In the soil zone (< 1 m in depth), measured NO_3^- -N concentration exhibited an increasing trend except for that in silty-loam during MLU. In specific, NO_3^- -N concentration increased by over three-fold down the vertical profile of silty-clay-loam during both WLU and MLU (Fig. 4c). In contrast, NO_3^- -N concentrations in the soil zone of silty-loam increased by 1.5-fold during MLU, but a reversed decreasing trend was observed for WLU (Fig. 3c).

In the subsoil zones (> 1 m in depth), however, measured NO_3^- -N concentration exhibited a decreasing trend except for that in silty-loam during WLU. Specifically, NO_3^- -N concentration decreased by over 90 %–70 % down the vertical profile of silty-clay-loam for WLU and MLU. While NO_3^- -N concentrations in the subsoil zone of silty-loam decreased by 70 % during MLU, but showed slight variation during WLU.

Moreover, a synchronous trend between Cl^- and NO_3^- -N was found in the correspondence subsoil zone of silty-loam as the $\text{NO}_3^-/\text{Cl}^-$ molar ratios varied slightly (Fig. 5b), but a decreasing trend of $\text{NO}_3^-/\text{Cl}^-$ was found in the subsoil zone of silty-clay-loam (Fig. 5a). This observation implied NO_3^- -N concentration in the subsoil zone of silty-loam was dominantly controlled by physical processes such as evaporation and rainfall dilution, but might be affected by biogeochemical processes in the subsoil zone of silty-clay-loam.

One of the observations was that measured VZ NO_3^- -N concentration during MLU was significantly higher than that of the WLU at both sites ($p < 0.001$, t test). This could be explained by the application of nitrogen fertilizer ($\sim 350 \text{ kg ha}^{-1}$) in late June before sowing the maize. Fertilizer-derived nitrogen might be flushed downward to the soil and subsoil zone, resulting in higher NO_3^- -N concentration in the VZ during MLU. Moreover, NO_3^- -N concentration in the VZ of silty-clay-loam was much higher than that of the silty-loam. This might be caused by the stratified texture of silty-clay-loam which hindered nitrate infiltration, resulting in higher nitrate accumulation in the VZ profile.

Meanwhile, measured groundwater NO_3^- -N concentration beneath silty-loam ($11.24 \pm 4.78 \text{ mg L}^{-1}$) was more than two times higher than that of the silty-clay-loam ($5.32 \pm 5.33 \text{ mg L}^{-1}$). This observation coincided with lower nitrate and TN retention in the VZ of silty-loam. Moreover, NO_3^- -N concentration of 3/4 groundwater samples beneath the silty-loam exceeded the drinking water quality limit (10 mg L^{-1} , EPA of China). In the silty-clay-loam area, however, only 2/14 of the groundwater samples exceeded this limit, suggesting higher groundwater vulnerability beneath the silty-loam.

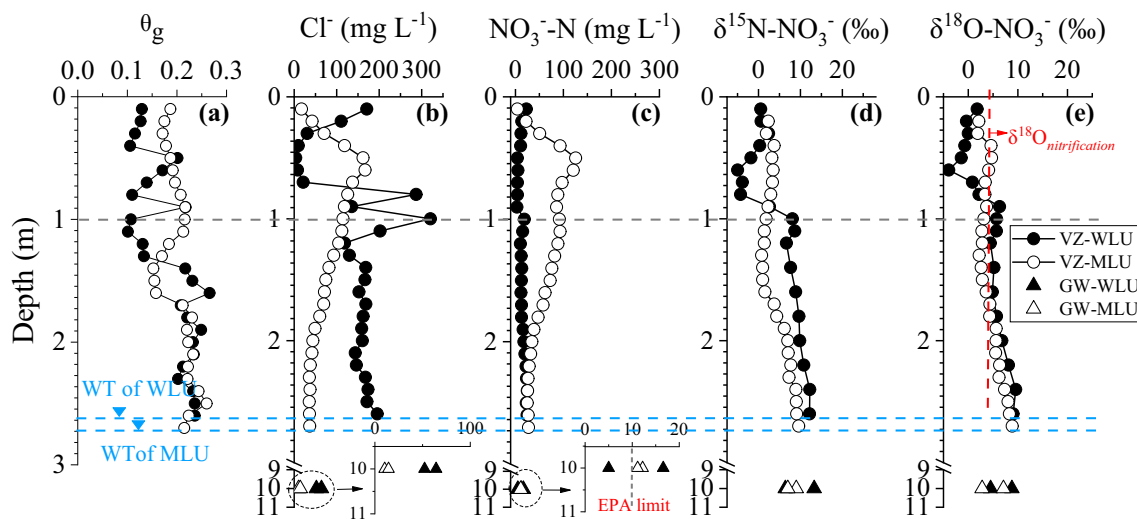


Fig. 3 Vertical profiles of **a** θ_g , **b** Cl^- , **c** NO_3^- -N, **d** $\delta^{15}\text{N-NO}_3^-$, **e** $\delta^{18}\text{O-NO}_3^-$ in the VZ and groundwater (GW) beneath silty-loam during the wheat land use (WLU) and maize land use (MLU). The vertical red dashed line stands for the theoretical $\delta^{18}\text{O-NO}_3^-$ derived from nitrification, and the horizontal blue dashed line stands for the water table (WT)

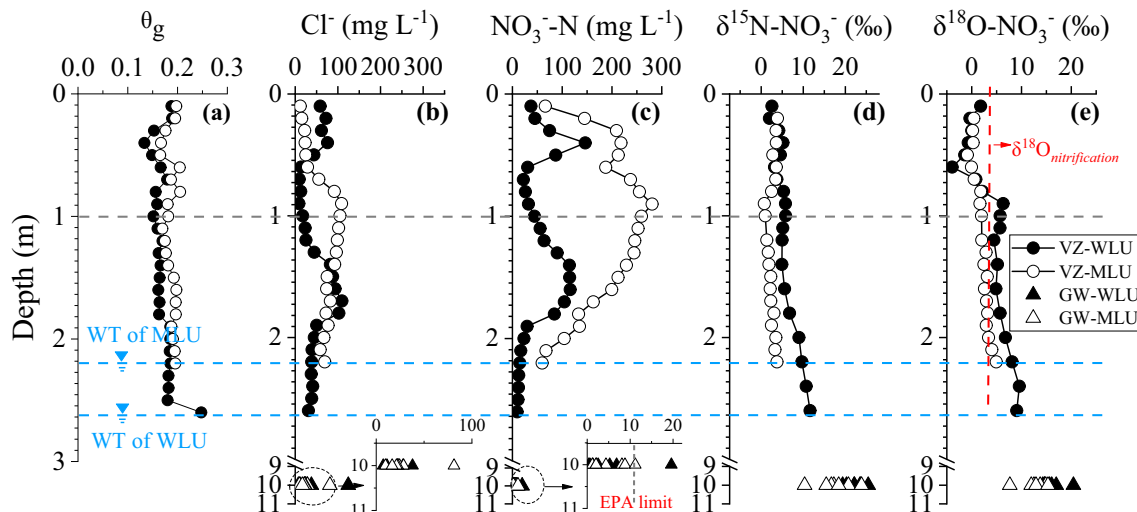


Fig. 4 Vertical profiles of **a** θ_g , **b** Cl^- , **c** NO_3^- -N, **d** $\delta^{15}\text{N-NO}_3^-$, **e** $\delta^{18}\text{O-NO}_3^-$ in the VZ and GW beneath silty-clay-loam during the wheat land use (WLU) and maize land use (MLU). The vertical red dashed line stands for the theoretical $\delta^{18}\text{O-NO}_3^-$ derived from nitrification, and the horizontal blue dashed line stands for the water table (WT)

3.3 Isotopic compositions of nitrate in VZ and groundwater

In the soil zones (< 1 m in depth), isotopic compositions of nitrate varied within narrow ranges at both sites. In specific, average $\delta^{15}\text{N-NO}_3^-$ and $\delta^{18}\text{O-NO}_3^-$ values were $0 \pm 3.9\text{ ‰}$, $1 \pm 3.1\text{ ‰}$ (WLU), $2.8 \pm 0.7\text{ ‰}$, $3.5 \pm 1.0\text{ ‰}$ (MLU) in the soil zone of silty-loam (Fig. 3d, e). In the soil zone of silty-clay-loam, $\delta^{15}\text{N-NO}_3^-$ and $\delta^{18}\text{O-NO}_3^-$ were $4.2 \pm 1.4\text{ ‰}$, $5.2 \pm 1.5\text{ ‰}$ (WLU), $2.8 \pm 1.2\text{ ‰}$, $0.7 \pm 1.0\text{ ‰}$ (MLU) respectively (Fig. 4d, e).

In the subsoil zones (> 1 m in depth), however, ^{15}N and ^{18}O were gradually enriched down the vertical profile at

both sites. Specifically, measured $\delta^{15}\text{N}$ and $\delta^{18}\text{O}$ enriched by 6.5 to 7.4 ‰ (WLU), and 3.0 to 3.2 ‰ (MLU) in subsoil zone of silty-clay-loam, and increased by 3.5 to 2.8 ‰ (WLU), and 7.8 to 2.0 ‰ (MLU) in subsoil zone of silty-loam.

Meanwhile, in silty-clay-loam area, groundwater NO_3^- was more rich with heavy isotopes ($\delta^{15}\text{N} = 19.9 \pm 4.1\text{ ‰}$, $\delta^{18}\text{O} = 14.4 \pm 2.9\text{ ‰}$) than those in the silty-loam area ($\delta^{15}\text{N} = 8.9 \pm 3.1\text{ ‰}$, $\delta^{18}\text{O} = 5.8 \pm 2.7\text{ ‰}$) (Table 1).

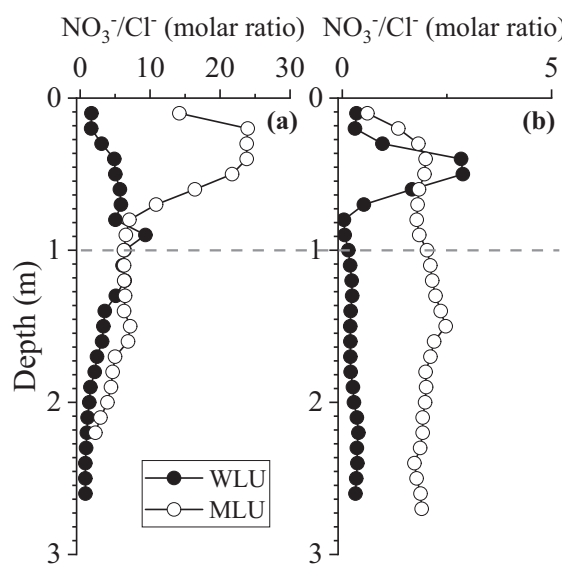


Fig. 5 Vertical profiles of $\text{NO}_3^-/\text{Cl}^-$ molar ratios in the VZ of a silty-clay-loam, and **b** silty-loam during the wheat land use (WLU) and maize land use (MLU)

4 Discussions

4.1 Nitrification in the vertical profile of the VZ

The traditional nitrification pathway suggests that 1/3 of the oxygen atoms in NO_3^- comes from atmospheric O_2 ($\delta^{18}\text{O}_{\text{air}} = 23.5 \text{ ‰}$), while the rest comes from the surrounding H_2O (Snider et al. 2010). Therefore, the theoretical $\delta^{18}\text{O}$ value ($\delta^{18}\text{O}_{\text{nitrification}}$) of nitrification-produced NO_3^- could be estimated based on the stoichiometric equation below:

$$\delta^{18}\text{O}_{\text{nitrification}} = 1/3\delta^{18}\text{O}_{\text{air}} + 2/3\delta^{18}\text{O}_{\text{soil water}} \quad (1)$$

In the study area, water in the soil zone (< 1 m in depth) was mainly derived from precipitation and groundwater irrigation. Due to the similarity of oxygen isotopic signature between rainwater ($\delta^{18}\text{O}_{\text{RW}} = -6.6 \text{ ‰}$) and groundwater ($\delta^{18}\text{O}_{\text{GW}} = -7.6 \text{ ‰}$ in the silty-loam area, and

-7.2 ‰ in the silty-clay-loam area), $\delta^{18}\text{O}_{\text{soil water}}$ was estimated using the average isotope value of rainwater and groundwater. As such, the $\delta^{18}\text{O}_{\text{nitrification}}$ was calculated to be 3.1 ‰ (soil zone of silty-loam) and 3.2 ‰ (soil zone of silty-clay-loam) based on Eq. (1). Measured $\delta^{18}\text{O}-\text{NO}_3^-$ values in the soil zones of silty-loam ($1.0 \pm 3.1 \text{ ‰}$ and $3.5 \pm 1.0 \text{ ‰}$) and silty-clay-loam ($5.2 \pm 1.5 \text{ ‰}$ and $0.7 \pm 1.0 \text{ ‰}$) varied around the $\delta^{18}\text{O}_{\text{nitrification}}$ values (Figs. 3e, 4e), suggesting the ubiquitous of nitrification in the soil zones regardless of soil types. The wider range of measured $\delta^{18}\text{O}-\text{NO}_3^-$ than the $\delta^{18}\text{O}_{\text{nitrification}}$ maybe explained by the isotopic fractionation of $\delta^{18}\text{O}_{\text{soil water}}$ and $\delta^{18}\text{O}_{\text{air}}$ caused by evaporation and root respiration (Xue et al. 2009).

The molar ratios of NO_3^- to Cl^- could verify the nitrification processes due to the inertness of Cl^- in biochemical reactions (Liu et al. 2006). In the soil zones, $\text{NO}_3^-/\text{Cl}^-$ gradually increased from 0.34 to 2.88 (WLU) and 0.60 to 1.99 (MLU) beneath the silty-loam, and increased from 1.62 to 9.35 (WLU) and from 14.19 to 23.96 (MLU) beneath the silty-clay-loam (Fig. 5). This observation implied the surplus of nitrate relative to chloride in the soil zone at both sites, further confirmed the occurrence of nitrification which contributed to soil nitrate pool. The ubiquitous nitrification process in the soil zones may facilitate nitrate leaching because of the higher mobility of nitrate in the VZ (Di and Cameron 2016).

4.2 Denitrification in the vertical profile of the VZ

4.2.1 Denitrification process identification

It is commonly realized that denitrifiers preferentially use light isotopes (^{14}N and ^{16}O), resulting in the enrichment of heavy isotopes (^{15}N and ^{18}O) in the residual nitrate pool along with the depletion of nitrate (Lehmann et al. 2003).

In the subsoil zone (> 1 m in depth) of silty-clay-loam, both $\delta^{15}\text{N}$ and $\delta^{18}\text{O}$ gradually increased (Fig. 4c, d) along with the dramatic decrease of $\text{NO}_3^-/\text{Cl}^-$ from 6.07 to 0.78

Table 1 Concentrations of DO, NO_3^- -N, isotopic compositions of NO_3^- and H_2O in groundwater beneath the silty-loam ($n = 4$), silty-clay-loam ($n = 14$), and rainwater ($n = 2$) during the study period

Sample ID	DO (mg L^{-1})	NO_3^- -N (mg L^{-1})	$\delta^{15}\text{N}-\text{NO}_3^- (\text{‰})$	$\delta^{18}\text{O}-\text{NO}_3^- (\text{‰})$	$\delta\text{D}-\text{H}_2\text{O} (\text{‰})$	$\delta^{18}\text{O}-\text{H}_2\text{O} (\text{‰})$
GW in site A ^a	4.74 ± 1.35	11.24 ± 4.78	8.9 ± 3.1	5.8 ± 2.7	-53.3 ± 2.9	-7.6 ± 0.6
GW in site B ^b	1.63 ± 0.77	5.32 ± 5.33	19.9 ± 4.1	14.4 ± 2.9	-51.5 ± 3.2	-7.2 ± 0.5
Rainwater	ND ^c	0.85 ± 0.86	7.8 ± 0.8	66.3 ± 1.8	-42.7 ± 3.6	-6.6 ± 0.3

Values were reported as mean \pm SD of n samples

^aSilty-loam

^bSilty-clay-loam

^cNot determined

(WLU) and from 6.28 to 2.19 (MLU) (Fig. 5a). In addition, the isotopic fractionation ratios of $\delta^{18}\text{O}$ to $\delta^{15}\text{N}$ were 1:1.2 ($p < 0.001$) during WLU and 1:1.1 ($p = 0.002$) during MLU (Fig. 6a), which were approximate to the reported denitrification isotope fractionation range of 1:1–1:2 (Hosono et al. 2013; Li et al. 2017). These findings demonstrably confirmed that denitrification was the dominant process leading to the enrichment of ^{15}N and ^{18}O in the subsoil zone of silty-clay-loam.

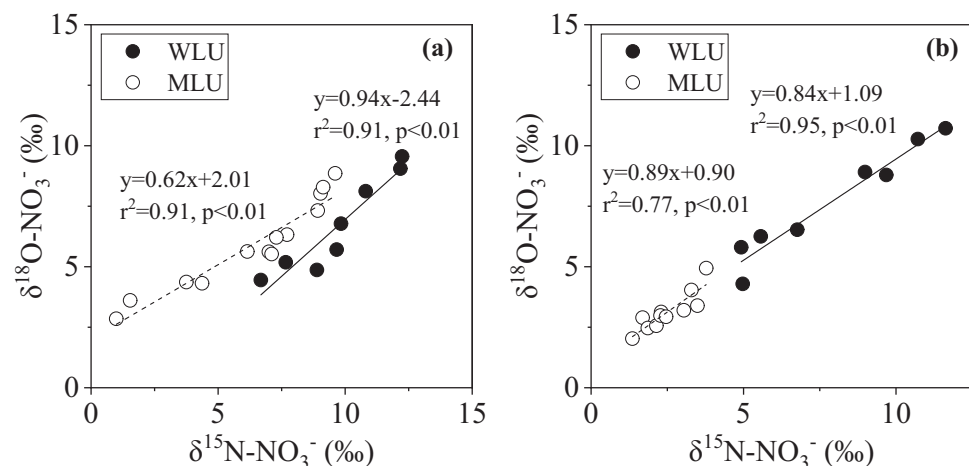
In the corresponding subsoil zone of silty-loam, both $\delta^{15}\text{N}$ and $\delta^{18}\text{O}$ increased slightly down the vertical profile regardless of crop types, with $\delta^{18}\text{O}$ to $\delta^{15}\text{N}$ fractionation ratios of 1:1.1 ($p < 0.001$) in WLU and 1:1.6 ($p < 0.001$) in MLU (Fig. 6b). On the contrary, no dramatic variations of $\text{NO}_3^-/\text{Cl}^-$ ratios were observed down the vertical profile (Fig. 5a). Specifically, in MLU, calculated $\text{NO}_3^-/\text{Cl}^-$ molar ratios decreased mildly from 2.47 to 1.73, but an inverse slightly increasing trend (from 0.04 to 0.39) was observed during WLU (Fig. 5b). These observations indicated that denitrification occurred during MLU but was absent during WLU.

4.2.2 Denitrification efficiency estimation

To further quantify the efficiency of denitrification in the subsoil zone, isotope enrichment factors (ε) of ^{15}N and ^{18}O during denitrification were estimated based on the linear relationships of $\delta^{15}\text{N}-\text{NO}_3^-$, $\delta^{18}\text{O}-\text{NO}_3^-$ and $\ln(\text{NO}_3^-/\text{Cl}^-)$ using the modified Rayleigh Equation (Li et al. 2018). The $\text{NO}_3^-/\text{Cl}^-$ molar ratios were used to eliminate the influence of physical processes (evaporation/precipitation) on nitrate concentration in the VZ.

$$\delta_{\text{sampling}} = \delta_{\text{initial}} - \varepsilon \cdot \ln \left(\frac{[\text{NO}_3^-/\text{Cl}^-]_{\text{sampling}}}{[\text{NO}_3^-/\text{Cl}^-]_{\text{initial}}} \right) \quad (2)$$

Fig. 6 Scatter plots of $\delta^{18}\text{O}-\text{NO}_3^-$ versus $\delta^{15}\text{N}-\text{NO}_3^-$ in the subsoil zone (> 1 m in depth) beneath **a** a silty-clay-loam, and **b** silty-loam during wheat land use (WLU) and maize land use (MLU)

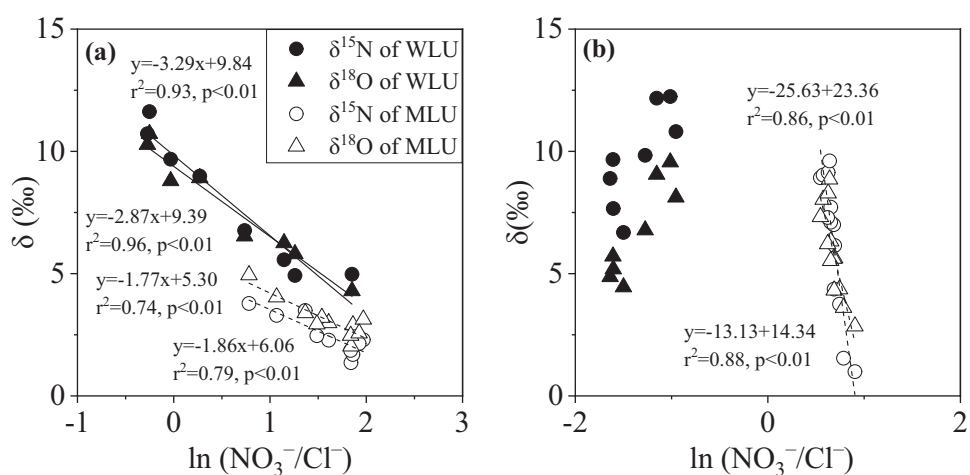


where δ_{sampling} and δ_{initial} are the isotopic compositions of nitrate at the sampling time and the initial time (when nitrate was formed and denitrification did not occur yet to affect the isotopic compositions of nitrate), ε stands for the isotope enrichment factor, and $[\text{NO}_3^-/\text{Cl}^-]_{\text{sampling}}$ and $[\text{NO}_3^-/\text{Cl}^-]_{\text{initial}}$ are $\text{NO}_3^-/\text{Cl}^-$ molar ratios at the sampling and initial time.

In the subsoil zone of silty-clay-loam, $\ln(\text{NO}_3^-/\text{Cl}^-)$ was significantly correlated to $\delta^{15}\text{N}-\text{NO}_3^-$ ($p < 0.001$) and $\delta^{18}\text{O}-\text{NO}_3^-$ ($p < 0.001$) of both land uses (Fig. 7a). Calculated ε values for ^{15}N and ^{18}O were 3.3 and 2.9 % (WLU), and 1.8 and 1.9 % (MLU) based on the Rayleigh distillation kinetics (i.e., a closed nitrate pool being consumed with a constant N-isotope effect) (Lehmann et al. 2007). In the corresponding subsoil zone of silty-loam, however, such linear correlations ($p < 0.001$) were only observed during MLU (Fig. 7b), and ε values for ^{15}N and ^{18}O were 25.6 and 13.1 % respectively.

Furthermore, the calculated ε values were used to estimate denitrification efficiency $(1 - \frac{[\text{NO}_3^-/\text{Cl}^-]_{\text{sampling}}}{[\text{NO}_3^-/\text{Cl}^-]_{\text{initial}}})$ using Eq. (2). The most depleted ^{15}N and ^{18}O ratios and high $\text{NO}_3^-/\text{Cl}^-$ molar ratios at the depth of 1.5 m in silty-loam VZ and 1.2 min silty-clay-loam VZ were assumed to represent the original isotopic compositions of nitrate (δ_{initial} in Eq. (2)) before denitrification. Calculations of the denitrification efficiency $(1 - \frac{[\text{NO}_3^-/\text{Cl}^-]_{\text{sampling}}}{[\text{NO}_3^-/\text{Cl}^-]_{\text{initial}}})$ based on Eq. (2) showed that as much as 76 %–88% of the total nitrate (mainly derived from nitrification end-product of fertilizer and soil nitrogen prior to denitrification) was removed during WLU and MLU via denitrification in the subsoil zone of silty-clay-loam. While in the subsoil zone of silty-loam, denitrification was only observed during MLU with the nitrate removal efficiency of 28 %. This difference in denitrification removal efficiency between silty-loam and

Fig. 7 Scatterplots of $\delta^{15}\text{N}-\text{NO}_3^-$ and $\delta^{18}\text{O}-\text{NO}_3^-$ versus $\ln(\text{NO}_3^-/\text{Cl}^-)$ in the subsoil zone ($> 1 \text{ m}$ in depth) of **a** silty-clay-loam and **b** silty-loam during the wheat land use (WLU) and maize land use (MLU)



silty-clay-loam profiles is in agreement with the observations of lesser groundwater nitrate problems under clayey vadose zones (Kurtzman et al. 2016).

4.2.3 Influencing factors of denitrification efficiency

The observed difference of denitrification efficiency in the subsoil zone between silty-loam and silty-clay-loam could be explained by the subsoil properties and VZ texture stratification. It's reported that nitrate concentration, electron donors, and redox conditions are the key factors controlling the denitrification process (Rivett et al. 2008; Zhou et al. 2017). In the subsoil zone of silty-clay-loam, NO_3^- -N concentrations (54.61 and 170.46 mg L⁻¹ during WLU and MLU) and OC (1.85%) were over two times higher than nitrate (16.97 and 49.59 mg L⁻¹ during WLU and MLU) and OC (0.81%) of silty-loam. Higher substrate content facilitated the denitrification process in the silty-clay-loam profile. Furthermore, compared with silty-loam VZ, the silty-clay-loam VZ with more vertical stratification might create anoxic interfaces beneficial for denitrifiers (Bradshaw and Radcliffe 2013).

4.3 Implications of VZ nitrogen transformations for groundwater quality

4.3.1 Groundwater nitrate sources identification

The fate of nitrogen in the VZ may significantly affect the groundwater quality (Spalding and Exner 1993; Yuan et al. 2012). In this study, measured $\delta^{18}\text{O}-\text{NO}_3^-$ signatures suggested that nitrate in the VZ beneath both soil types was mainly derived from the nitrification end-product of nitrogen fertilizer and soil nitrogen (Fig. 8).

In the groundwater beneath the silty-loam, measured $\delta^{15}\text{N}-\text{NO}_3^-$ and $\delta^{18}\text{O}-\text{NO}_3^-$ ($\delta^{15}\text{N}_{\text{mean}} = 8.9 \text{ ‰}$, $\delta^{18}\text{O}_{\text{mean}} = 5.8 \text{ ‰}$) were similar to those at the bottom of the

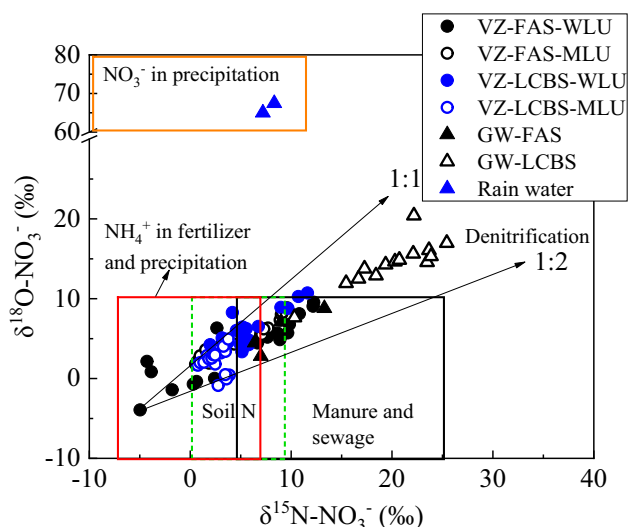


Fig. 8 Cross-plots of $\delta^{18}\text{O}-\text{NO}_3^-$ versus $\delta^{15}\text{N}-\text{NO}_3^-$ in the vadose zone (VZ), groundwater (GW), rainwater, and various nitrate sources. WLU and MLU represent wheat land use and maize land use, respectively. Two dashed lines with arrows represent $\delta^{18}\text{O}$ to $\delta^{15}\text{N}$ fractionation ratios of 1:1 and 1:2 during denitrification. The boxes represent the isotopic compositions of various nitrate sources modified from Xue et al. (2009)

VZ (Fig. 3c, d), denoting that groundwater nitrate was mainly derived from VZ leaching recharge. In the groundwater beneath the silty-clay-loam, however, isotopic compositions of nitrate ($\delta^{15}\text{N}_{\text{mean}} = 19.9 \text{ ‰}$, $\delta^{18}\text{O}_{\text{mean}} = 14.4 \text{ ‰}$) were two times higher than those at the bottom of the VZ, indicating that the VZ leaching-derived nitrate had also undergone intensive denitrification in the aquifer. Higher denitrification potential in the groundwater beneath silty-clay-loam may be explained by lower DO concentration (1.63 mg L⁻¹) than that beneath silty-loam (4.74 mg L⁻¹) (Rivett et al. 2008).

4.3.2 Groundwater nitrate vulnerability and its influencing factors

Groundwater NO_3^- -N concentration beneath silty-loam was over two times higher than that in silty-clay-loam (11.24 mg L^{-1} vs. 5.32 mg L^{-1}), while average NO_3^- -N concentrations in the VZ of silty-loam (14.22 and 60.09 mg L^{-1}) were much lower than those of silty-clay-loam (54.61 and 187.13 mg L^{-1}). This might be explained by that groundwater nitrate vulnerability was not only correlated to NO_3^- -N concentration in VZ, but also determined by water percolation rate which was affected by precipitation, VZ texture and materials (Green et al. 2008). Higher sand content and lower clay content of the silty-loam resulted in higher permeability, which could promote water percolation and nitrate leaching processes in the VZ (Green et al. 2008; Bradshaw and Radcliffe 2013).

Moreover, it's conceivable that the total nitrogen input (fertilizer, N precipitation, and N fixation) at two sites of the study area was approximately the same under the same land use. In the VZ of silty-loam, however, both denitrification efficiency and nitrogen retention (estimated as TN in Fig. 2c) were lower than those in the VZ of silty-clay-loam, resulting in higher nitrate leaching risk in silty-loam. Hence, it could be concluded that groundwater beneath the silty-loam VZ was more vulnerable due to the inactive denitrification and high permeability caused by OC-poor, coarse soil particles, and loose texture. While in-situ nitrate leaching flux of various soil types under global climate change should be simulated in further studies to provide quantitative guidance for rational fertilization.

5 Conclusions

Multi-isotope tracers were used to probe the behavior of fertilizer-derived nitrogen in the VZ-groundwater continuum, and to analyze the implications for groundwater vulnerability and rational fertilization in silty-loam and silty-clay-loam soils in the Huaihe River Basin. (1) Measured $\delta^{18}\text{O}-\text{NO}_3^-$ value in the soil zone ($< 1 \text{ m}$ in depth) was similar to the theoretical value of nitrification in all examined scenarios, indicating nitrification was the main nitrogen transformation pathway. In the subsoil zone ($> 1 \text{ m}$ in depth), however, the occurrence of denitrification was evidenced by the enrichment of ^{15}N and ^{18}O in nitrate along with the decrease of $\text{NO}_3^-/\text{Cl}^-$ molar ratios. (2) Further quantitative analysis showed that denitrification removed as much as 76 %–88 % of the total nitrate in the OC-rich silty-clay-loam VZ with stratified texture, compared with 0 %–28 % nitrate removal efficiency in the OC-depleted silty-loam VZ with a uniform texture. (3) Inactive denitrification along with high permeability silty-loam

suggested higher nitrate leaching risk. Furthermore, groundwater NO_3^- -N concentration (11.24 mg L^{-1}) beneath the silty-loam was as much as two times higher than that of the silty-clay-loam (5.32 mg L^{-1}). These observations indicated that groundwater beneath the OC-depleted coarse-particle soil with the uniform texture was more vulnerable to nitrate pollution. Hence, stricter fertilization management strategies should be applied.

Acknowledgements This work was supported by the Key Program of the National Natural Science Foundation of China (41230640) and Major Science and Technology Program for Water Pollution Control and Treatment (2017ZX07602003).

Compliance with ethical standards

Conflict of interest On behalf of all authors, the corresponding author states that there is no conflict of interest.

References

- Ascott MJ, Goody DC, Wang L, Stuart ME, Lewis MA, Ward RS, Binley AM (2017) Global patterns of nitrate storage in the vadose zone. *Nat Commun* 8:1416
- Baram S, Arnon S, Ronen Z, Kurtzman D, Dahan O (2012) Infiltration mechanism controls nitrification and denitrification processes under dairy waste lagoon. *J Environ Qual* 41:1623–1632
- Bonde TA, Lindberg T (1988) Nitrogen mineralization kinetics in soil during long-term aerobic laboratory incubations: a case study. *J Environ Qual* 17:414–417
- Bradshaw JK, Radcliffe DE (2013) Nitrogen fate and transport in a conventional onsite wastewater treatment system installed in a clay soil: experimental results. *Vadose Zone J* 12:1–20
- Bünemann EK, Bongiorno G, Bai Z et al (2018) Soil quality—a critical review. *Soil Biol Biochem* 120:105–125
- Casciotti KL, Sigman DM, Hastings MG, Bohlke JK, Hilkert A (2002) Measurement of the oxygen isotopic composition of nitrate in seawater and freshwater using the denitrifier method. *Anal Chem* 74:4905–4912
- Denk TRA, Mohn J, Decock C, Lewicka-Szczebak D, Harris E, Butterbach-Bahl K, Kiese R, Wolf B (2017) The nitrogen cycle: a review of isotope effects and isotope modeling approaches. *Soil Biol Biochem* 105:121–137
- Di HJ, Cameron KC (2016) Inhibition of nitrification to mitigate nitrate leaching and nitrous oxide emissions in grazed grassland: a review. *J Soils Sediments* 16:1–20
- Donner SD, Kucharik CJ (2003) Evaluating the impacts of land management and climate variability on crop production and nitrate export across the Upper Mississippi Basin. *Glob Biogeochem Cycles* 17:1085
- González-Delgado AM, Shukla MK (2011) Coupled transport of nitrate and chloride in soil columns. *Soil Sci* 176:346–355
- Gray JM, Humphreys GS, Deckers JA (2011) Distribution patterns of World Reference Base soil groups relative to soil forming factors. *Geoderma* 160:373–383
- Green CT, Fisher LH, Bekins BA (2008) Nitrogen fluxes through unsaturated zones in five agricultural settings across the United States. *J Environ Qual* 37:1073–1085
- Gu B, Ge Y, Chang SX, Luo W, Chang J (2013) Nitrate in groundwater of China: Sources and driving forces. *Glob Environ Change* 23:1112–1121

- Holden PA, Fierer N (2005) Microbial processes in the vadose zone. *Vadose Zone J* 4:1–21
- Hosono T, Tokunaga T, Kagabu M, Nakata H, Orishikida T, Lin IT, Shimada J (2013) The use of $\delta^{15}\text{N}$ and $\delta^{18}\text{O}$ tracers with an understanding of groundwater flow dynamics for evaluating the origins and attenuation mechanisms of nitrate pollution. *Water Res* 47:2661–2675
- Izbicki JA, Flint AL, O'Leary DR, Nishikawa T, Martin P, Johnson RD, Clark DA (2015) Storage and mobilization of natural and septic nitrate in thick unsaturated zones, California. *J Hydrol* 524:147–165
- Jia X, Zhu Y, Huang L, Wei X, Fang Y, Wu L, Binley A, Shao M (2018) Mineral N stock and nitrate accumulation in the 50 to 200 m profile on the Loess Plateau. *Sci Total Environ* 633:999–1006
- Koper TE, Stark JM, Habteselassie MY, Norton JM (2010) Nitrification exhibits Haldane kinetics in an agricultural soil treated with ammonium sulfate or dairy-waste compost. *FEMS Microbiol Ecol* 74:316–322
- Kurtzman D, Baram S, Dahan O (2016) Soil-aquifer phenomena affecting groundwater under vertisols: a review. *Hydrol Earth Syst Sci* 20:1–12
- Lehmann MF, Reichert P, Bernasconi SM, Barbieri A, McKenzie JA (2003) Modelling nitrogen and oxygen isotope fractionation during denitrification in a lacustrine redox-transition zone. *Geochim Cosmochim Acta* 67:2529–2542
- Lehmann MF, Sigman DM, McCorkle DC, Granger J, Hoffmann S, Cane G, Brunelle BG (2007) The distribution of nitrate $^{15}\text{N}/^{14}\text{N}$ in marine sediments and the impact of benthic nitrogen loss on the isotopic composition of oceanic nitrate. *Geochim Cosmochim Acta* 71:5384–5404
- Li R, Ruan X, Bai Y, Ma T, Liu C (2017) Effect of wheat-maize straw return on the fate of nitrate in groundwater in the Huaihe River Basin, China. *Sci Total Environ* 592:78–85
- Li C, Li SL, Yue FJ, Liu J, Zhong J, Yan ZF, Zhang RC, Wang ZJ, Xu S (2018) Identification of sources and transformations of nitrate in the Xijiang River using nitrate isotopes and Bayesian model. *Sci Total Environ* 646:801–810
- Liu CQ, Li SL, Lang YC, Xiao HY (2006) Using $\delta^{15}\text{N}$ - and $\delta^{18}\text{O}$ -values to identify nitrate sources in karst ground Water, Guiyang, southwest China. *Environ Sci Technol* 40:6928–6933
- Liu B, Morkved PT, Frostegard A, Bakken LR (2010) Denitrification gene pools, transcription and kinetics of NO, N_2O and N_2 production as affected by soil pH. *FEMS Microbiol Ecol* 72:407–417
- McMahon PB, Dennehy KF, Bruce BW, Böhlke JK, Michel RL, Gurdak JJ, Hurlbut DB (2006) Storage and transit time of chemicals in thick unsaturated zones under rangeland and irrigated cropland, High Plains, United States. *Water Resour Res* 42:W03413
- Rasse DP, Ritchie JT, Peterson WR, Wei J, Smucker AJM (2000) Rye cover crop and nitrogen fertilization effects on nitrate leaching in inbred maize fields. *J Environ Qual* 29:298–304
- Rivett MO, Buss SR, Morgan P, Smith JW, Bemment CD (2008) Nitrate attenuation in groundwater: a review of biogeochemical controlling processes. *Water Res* 42:4215–4232
- Sigman DM, Casciotti KL, Andreani M, Barford C, Galanter M, Böhlke JK (2001) A bacterial method for the nitrogen isotopic analysis of nitrate in seawater and freshwater. *Anal Chem* 73:4145–4153
- Singh G, Kaur G, Williard K, Schoonover J, Kang J (2018) Monitoring of water and solute transport in the vadose zone: a review. *Vadose Zone J* 17:160058
- Snider DM, Spoelstra J, Schiff SL, Venkiteswaran JJ (2010) Stable oxygen isotope ratios of nitrate produced from nitrification: (^{18}O) -labeled water incubations of agricultural and temperate forest soils. *Environ Sci Technol* 44:5358–5364
- Spalding RF, Exner ME (1993) Occurrence of nitrate in groundwater—a review. *J Environ Qual* 22:392–402
- Stumpp C, Bruggemann N, Wingate L (2018) Stable isotope approaches in vadose zone research. *Vadose Zone J* 17:180096
- Xue D, Botte J, De Baets B, Accoe F, Nestler A, Taylor P, Van Cleemput O, Berglund M, Boeckx P (2009) Present limitations and future prospects of stable isotope methods for nitrate source identification in surface- and groundwater. *Water Res* 43:1159–1170
- Yuan L, Pang Z, Huang T (2012) Integrated assessment on groundwater nitrate by unsaturated zone probing and aquifer sampling with environmental tracers. *Environ Pollut* 171:226–233
- Zhang C-Y, Zhang S, Yin M-Y, Ma L-N, He Z, Ning Z (2012) Nitrogen isotope studies of nitrate contamination of the thick vadose zones in the wastewater-irrigated area. *Environ Earth Sci* 68:1475–1483
- Zhou W, Xia L, Yan X (2017) Vertical distribution of denitrification end-products in paddy soils. *Sci Total Environ* 576:462–471
- Zhu G, Wang S, Wang C, Zhou L, Zhao S, Li Y, Li F, Jetten MSM, Lu Y, Schwark L (2018) Resuscitation of anammox bacteria after $\approx 30,000$ years of dormancy. *ISME J* 13:1098–1109